

Mountain shadow phenomena. 2: The spike seen by an off-summit observer

David K. Lynch

The oblique spike or contrast edge seen by an off-summit observer on a mountain shadow when the sun is low is shown to be a perspective effect that depends on the observer's position within the shadow. The degree of visibility of the shadow is due to contrast effects between differently illuminated aerosols. Numerical simulations are used to demonstrate these points.

I. Introduction

Mountain shadows viewed from the summit have a characteristic triangular shape regardless of the mountain's true profile. This has been discussed by Livingston and Lynch,¹ who developed a first-order theory to account for the shape. By geometry the observer sees the shadow below the horizon. An observer who is below the summit and inside the shadow sees the triangular shadow as before but also sees a spike extending obliquely up and away (Fig. 1). Depending on the clarity of the air, this phenomenon may also appear as a contrast edge, i.e., a dark band that is sharp on one side and diffuse on the other. We shall refer to it as the spike throughout the rest of the paper. The spike stretches above the horizon many degrees and occurs on the side of the shadow away from the observer. Thus an observer on the left side of a mountain (looking toward the shadow) sees the spike pointing away on the right side of the shadow and vice versa. The fact that it can be seen above the horizon means that the shadow is actually cast on the air and is visible by virtue of airborne aerosols. The purpose of this study is to explain quantitatively the origin and contrast of the mountain shadow and its spike.

II. Geometrical Model

In this study it is assumed that the visibility of the shadow is due to differences in scattering between shadowed and unshadowed aerosols. Since the contrast depends on contributions from each regime integrated along the line of sight, the important quantity to mea-

sure or calculate is the path luminance or, conversely, the path length in the shadow along the line of sight.

The geometry of shadow formation is shown in Fig. 2(a). Observer O located on a conical mountain looks in directions a (azimuth) and e (elevation). His line of sight intersects the shadow boundary at D , and the path length through the shadow is OD . For simplicity a mountain whose cross section is triangular was used in the model, though as we know, the shadow of any mountain is triangular regardless of its true profile. Three planes limit the apparent path length by defining the edges of the shadow; the ground plane (B_1, B_2, P), the right penumbral plane (B_1, S, P), and the left penumbral plane (B_2, S, P). The altitude of the sun affects the location of P and also is a factor in determining the shadow geometry.

III. Numerical Calculations

To calculate path length OD , the following steps were taken:

(1) Define the circumstances: solar altitude α , base-to-height ratio of the mountain, and observer location.

(2) Calculate the equation of the line through O with azimuth a and elevation e .

(3) Calculate the equations of the three planes bordering the shadow.

(4) Calculate the point where the line intersects the three planes.

(5) Determine whether these points are within one of the triangles (B_1, B_2, P), (B_1, S, P), or (B_2, S, P).

(6) Determine which point of intersection is closest to O but which still lies in the a, e direction to avoid a plane-line intersection point that satisfies the proximity criterion but which is behind the observer, i.e., away from the shadow. This happens whenever the observer is located inside the shadow.) This point is D .

(7) Calculate path length OD .

The author is with Hughes Research Laboratories, Malibu, California 90265.

Received 22 December 1979.

0003-6935/80/101585-05\$00.50/0.

© 1980 Optical Society of America.

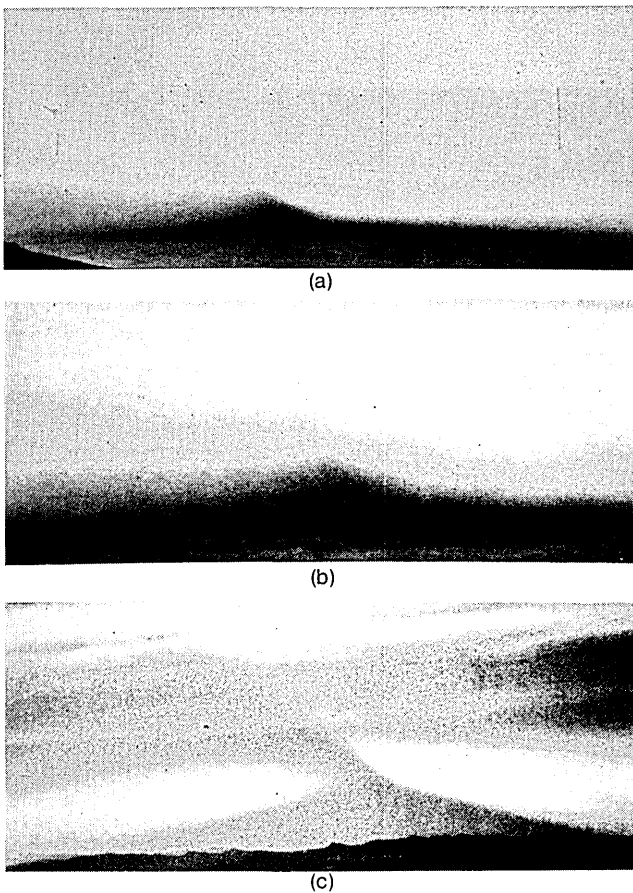


Fig. 1. Spikes observed on mountain shadows: (a) Pico del Teide, M. Cohen; (b) Pico del Teide, L. Cox; (c) Popocatepetl, D. K. Lynch.

For all calculations the base-to-height ratio of the mountain is 4, and unless otherwise indicated the solar altitude is 2° . The sun is assumed to be a point source. For display purposes path length OD is subtracted from a large number to reverse the contrast, thereby making comparisons with Fig. 1 easier. Each picture is 60° wide, 20° high, and centered on $a = 0$ (toward $+y$), $e = 0$ as seen by the observer who is located on the right side of the mountain ($x > 0$). In the following discussions we shall refer to the penumbral planes viewed by the observer as apparent penumbral planes.

Figure 2(b) shows the geometry of the shadow as viewed from directly above the summit. The numbered positions refer to the observer's x - y locations. The z position is the intersection of a vertical line through the location and the conical surface defining the mountain. The sequences of shadows seen from (1, 2, 3, 4, and 5), (1, 6, 7, 8, and 9), and (1, 10, 11, 12, and 13) are shown in Figs. 3, 4, and 5, respectively.

Figure 3 shows the shadows seen by observers on the right-hand terminator of the mountain. The first image [Figs. 3(a), 4(a), and 5(a)] shows the shadow as seen from the summit. It displays the properties discussed by Livingston and Lynch¹ including the apex angle $2 \tan^{-1}(b/2) = 127^\circ$, where b is the base-to-height ratio which is 4 in this case. The shadow appears darkest

near the mountain's summit because of the rapidly increasing path length as the elevation of the line of sight approaches $-\alpha$ from below, i.e., the apex where the path length approaches its maximum value of $Z/\sin\alpha$. The edges of the shadow appear sharp because the observer's line of sight lies in the plane between shadow and sunlight, and, consequently, an infinitesimal change in viewing angle carries the line of sight completely across the shadow boundary. This effect is slightly enhanced in this simulation because a point source of light casts no penumbra. Both sides of the shadow are identical, resulting from the obvious symmetry of the observer's location with respect to the penumbral planes.

As the observer moves down the mountain along the terminator [Figs. 3(b), (c), and (d)] several effects develop. The shadow boundary opposite the observer (left

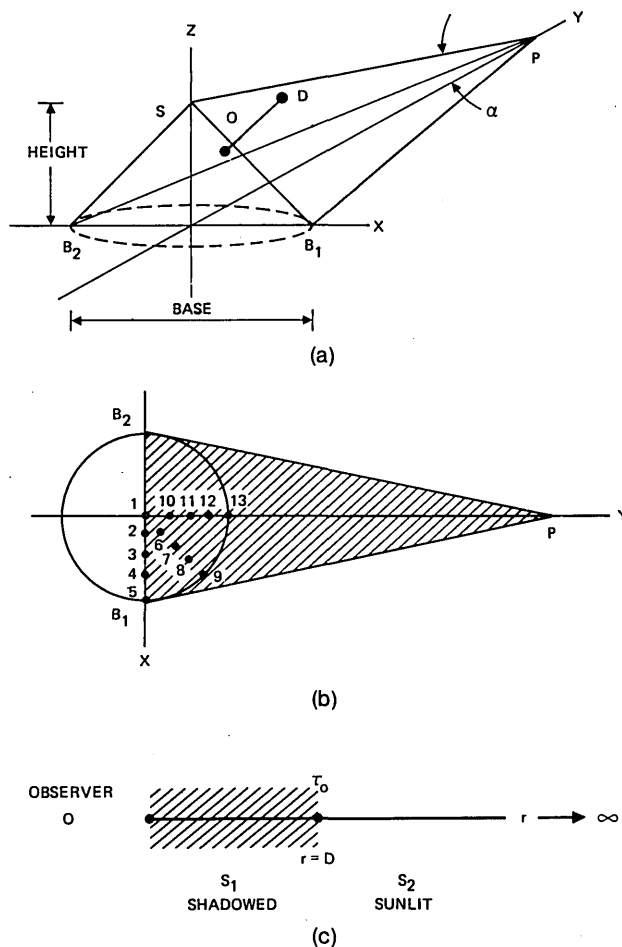


Fig. 2. Geometry of shadow formation. (a) Perspective view of the circumstances of the shadow. Observer O located in the right penumbral plane SB_1Y looks through the shadow where his line of sight intersects the left penumbral plane SB_2Y at D . The elevation of the sun is α . (b) Downward view of the shadow. Location at which calculations were made: Fig. 3—(1, 2, 3, 4, and 5); Fig. 4—(1, 6, 7, 8, and 9); Fig. 5—(1, 10, 11, 12, and 13); Fig. 6—(2); Fig. 7—(6); Fig. 8—(10). (c) Optical depth considerations. Observer O looks through the shaded region with source function S_1 to the unshaded region with source function S_2 . Distance OD is characterized by optical depth τ_0 .

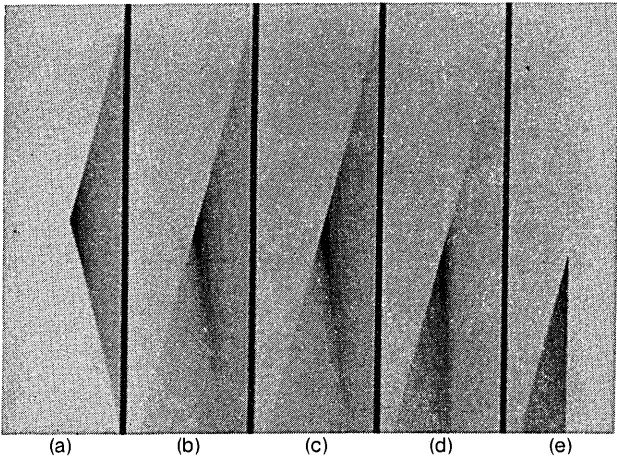


Fig. 3. Shadow observed along the right terminator of the mountain for solar elevation $\alpha = 2^\circ$. As the observer moves down the mountain, the shadow becomes less symmetric, loses the clarity of the apparent opposite penumbral plane, and the apex angle increases. Note that the upper boundary of the shadow above the apparent left penumbral plane is a linear extension of the observer's right penumbral plane.

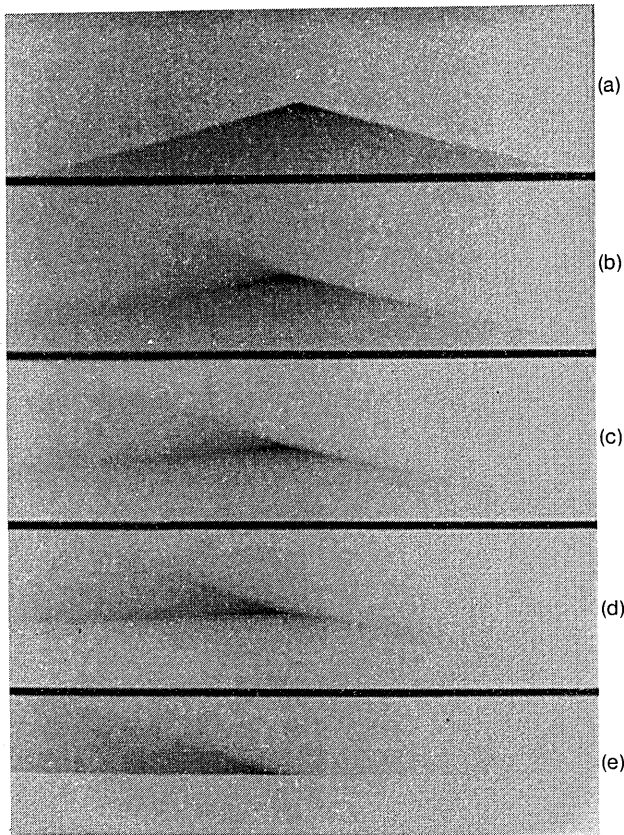


Fig. 4. Spike observed from within but off $x = 0$. As the observer moves down the mountain, the spike develops as an oblique shadow coming from the apparent shadow summit. Its upper boundary is not a linear extension of the right penumbral plane as in Fig. 3.

side) becomes less distinct because his line of sight crosses the penumbral plane obliquely and integrates varying amounts of shaded and unshaded sky. The previously unshaded region of the sky above the left apparent penumbral plane (shadow boundary) shows a shadow, and near the apparent summit it looks like a geometrical precursor to the spike. The apex angle increases because the apparent penumbral plane on the left becomes more and more horizontal, eliminating the symmetry. The observer's penumbral plane now extends upward, because he is located below the summit. Since he is always coplanar with the right penumbral plane, the upper boundary appears as a linear extension of that plane. When the observer is on the ground plane at $B1$ [Fig. 3(e)], the entire shadow is off to the left, and the apparent left penumbral plane has become horizontal, its lower edge now sharp because it has coalesced with the ground plane.

Figure 4 shows a similar sequence of mountain shadows for observers located on the mountain and within the shadow itself. The gross morphological properties of the shadow are the same as before with two important exceptions. Since the observer is no longer in the right penumbral plane, there is a discontinuity

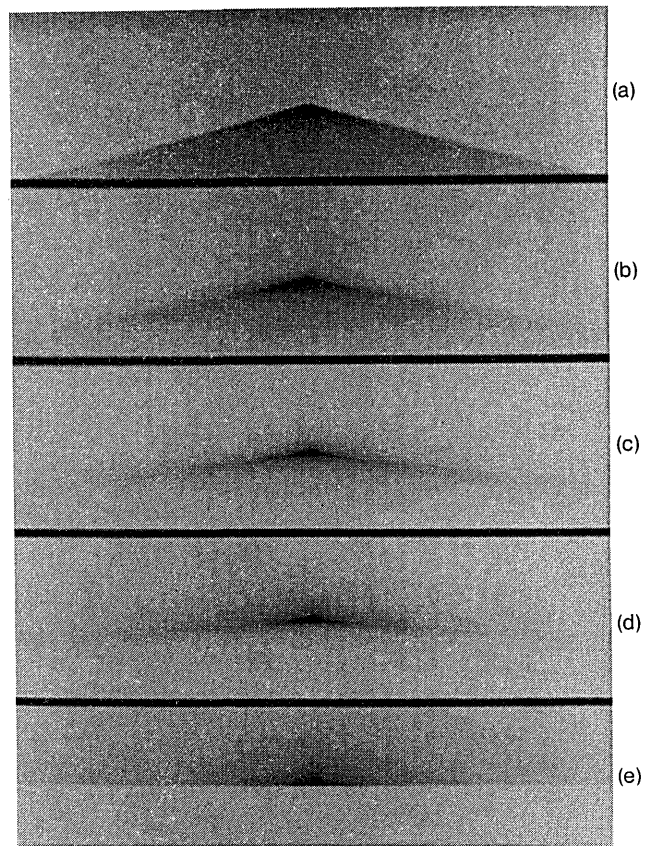


Fig. 5. Shadow observed from within with $x = 0$. The obvious symmetry causes the left and right penumbral planes to lose their sharpness together as the observer moves down the mountain.

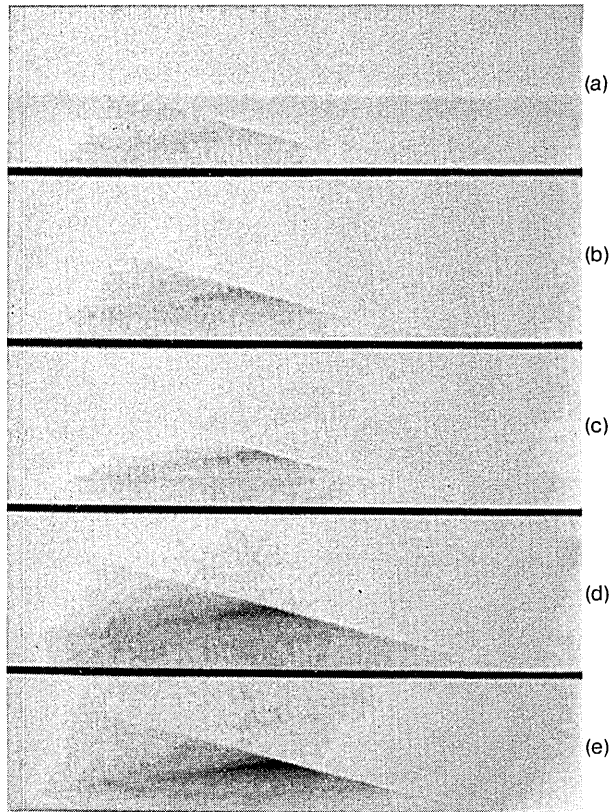


Fig. 6. Shadow and spike from location 2 for $\alpha = 10, 8, 6, 4,$ and $2.$

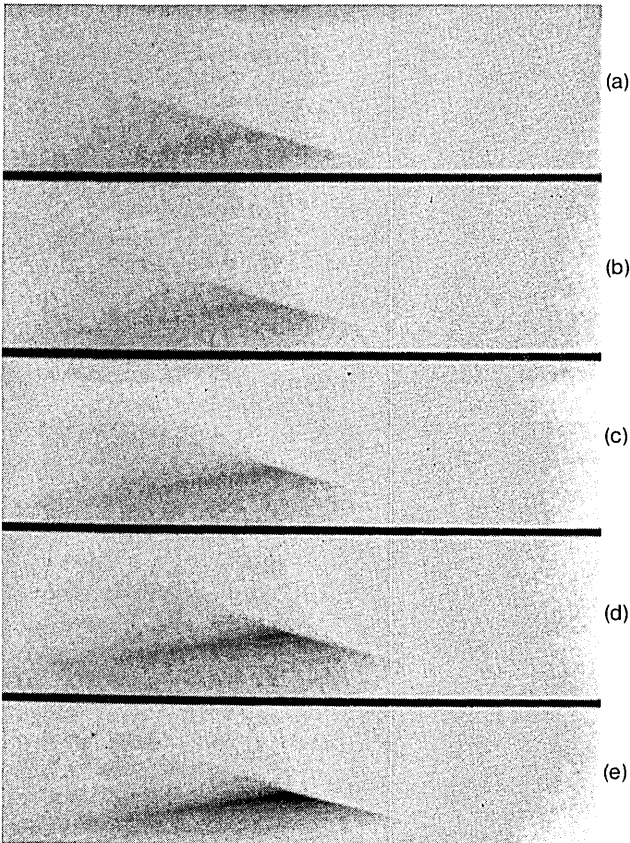


Fig. 7. Shadow and spike from location 6 for $\alpha = 10, 8, 6, 4,$ and $2.$

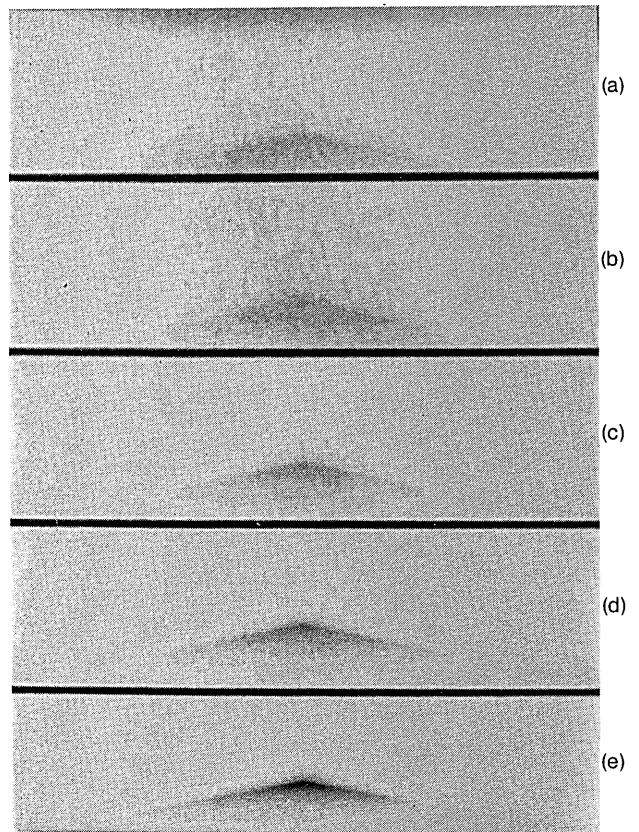


Fig. 8. Shadow and spike from location 10 for $\alpha = 10, 8, 6, 4,$ and $2.$

in the upper limit of the shadow above the left penumbral plane. We identify this part of the shadow as the spikes shown in Fig. 1. Figure 4(b) most closely resembles Figs. 1(a) and (c). As expected, neither shadow boundary is distinct now. Figure 4(e) shows the shadow as it appears from the base of the mountain. Since the observer is still within the shadow, it appears to surround him.

Figure 5 shows the shadow as it appears for observers located on the mountain for $x = 0$. Moving down from the summit [Fig. 5(a)], the most obvious effects are the simultaneous increase in the apex angle and the decrease in sharpness of the apparent penumbral planes. The symmetry is apparent. The spike some people see in Fig. 5 is not real but is only a contrast effect as an examination of the numerical data revealed. Rule (2) in Ref. 1 states that the "apex angle of the shadow . . . is independent of the observer's position." This is true to first order, especially when the observer is near the summit as considered by Livingston and Lynch. However, this analysis reveals that changes in the observer's location on a scale comparable with the size of the mountain produce significant changes in the apex angle.

Another interesting series of images can be made by keeping the observer in one position and letting the altitude of the sun change. This is shown in Figs. 6, 7, and 8. From top to bottom the altitude of the sun is 10, 8, 6, 4, and 2°. The locations of the observers in Figs. 6, 7, and 8 are 2, 6, and 10, respectively. Clearly the contrast of the shadow is a strong function of solar altitude, varying roughly with path length, which varies with $csc\alpha$ as noted before. For this reason the shadow is seldom seen when the sun is high in the sky, even if the slope of the mountain flank is greater than α .

IV. Visibility and Contrast

Let us theoretically consider the illumination through a shadow. Figure 2(c) shows the observer's line of sight through a shadow and beyond. There are two source functions S_1 and S_2 that characterize the amount of energy scattered toward the observer. Although we assume that the concentration of scatterers is the same in both regions, the illumination is not the same, and this causes the contrast. In the shadow (S_1) the energy comes from multiple scattering of skylight. In the sunlit portion there is an additional contribution from single scattering of sunlight that dominates S_2 . Light passing through the scattering region suffers an extinction (both scattering and absorption), and the observer sees a luminance L_1

$$L_1 = \int_0^{\tau_0} S_1 \exp(-\tau) d\tau + \int_{\tau_0}^{\infty} S_2 \exp(-\tau) d\tau, \quad (1)$$

where τ is the broadband optical depth, which may be defined in a number of ways, such as

$$\tau = \int_0^D n k d r,$$

where n is the density of scatterers (cm^{-3}), and k is the absorption coefficient per scatterer (cm^2). The luminance observed outside the shadow is L_2 :

$$L_2 = \int_0^{\infty} S_2 \exp(-\tau) d\tau = \int_0^{\tau_0} S_2 \exp(-\tau) d\tau + \int_{\tau_0}^{\infty} S_2 \exp(-\tau) d\tau. \quad (2)$$

Contrast C between the shaded and unshaded regions is

$$C = \frac{L_1 - L_2}{L_2}. \quad (3)$$

Substituting Eqs. (1) and (2) into Eq. (3) and integrating, we find

$$C = \frac{S_1 - S_2}{S_2} [1 - \exp(-\tau_0)].$$

For $\tau_0 \gg 1$,

$$C = \frac{S_1 - S_2}{S_2},$$

and for $\tau_0 \ll 1$,

$$C = \left(\frac{S_1 - S_2}{S_2} \right) \tau_0.$$

Clearly if $\tau_0 = 0$ (clear air) or $S_1 = S_2$ (no shadow), the contrast is zero.

Most scattering functions² decrease rapidly with scattering angle, reaching a minimum at ~ 80 – 120° . For an observer in the shadow, 90° elevation corresponds roughly to the shortest path length. The resulting small τ_0 and low scattering efficiency should cause the spike to be nearly invisible overhead, which agrees with the observations.

The previous discussion assumed that S_1 and S_2 are spatially uniform. However, the vertical distribution of aerosols is far from constant. For a well-mixed atmosphere, the aerosol scale height of 3.6 km (Ref. 3) is far less than the atmospheric scale height of 10 km (Ref. 4) but still comparable with the height of the mountain. Consequently, the contribution from the lower layers of the shadow may be stronger than those from the upper parts. Again this would alter the visibility of the shadow. In some cases the aerosol concentration may show inversions because various layers are present within the shadow. Such a situation could lead to remarkable contrast variations in the spike and shadow as Fig. 1(c) suggests.

The author is pleased to thank W. C. Livingston and R. L. Forward for their helpful discussions during this work and M. Cohen and L. Cox for allowing him to use the photographs in Fig. 1.

References

1. W. C. Livingston and D. K. Lynch, *Appl. Opt.* **18**, 265 (1979).
2. D. Deirmendjian, *Appl. Opt.* **3**, 187 (1964).
3. L. Elterman, AFCRL Report 68-0153 (AFCRL, Bedford, Mass., 1968).
4. United States Standard Atmosphere, NAS 1.2:At6/962 (U.S. GPO, Washington, D.C., 1962).